Biogeochemistry (2014) 121:565–580
DOI 10.1007/s10533-014-0023-x

Stable isotopic evidence of enhanced export of microbially derived NO_3^- following active layer slope disturbance in the Canadian High Arctic

Nicole L. Louiseize · Melissa J. Lafrenière · Meredith G. Hastings

Received: 2 May 2014 / Accepted: 7 August 2014 / Published online: 23 August 2014

Abstract Permafrost disturbance is expected to alter nitrogen (N) export in High Arctic watersheds by enhancing loads of dissolved inorganic N (DIN), particularly nitrate (NO_3^-), by enabling nitrification and/or the mobilization of N previously sequestered in deeper permafrost soils. Using chemical, isotopic, and hydrologic measurements, we compare the seasonal evolution of concentrations and sources of NO_3^- in a stream draining an undisturbed catchment with one that drains a catchment that has been affected by active layer detachments (ALDs) at the Cape Bounty Arctic Watershed Observatory (74°54′N, 109°35′W) on Melville Island, Nunavut. Oxygen stable isotope values of NO_3^- ($\delta^{18}O\text{-}NO_3^-$) from streamwater indicate that NO_3^- in runoff predominantly originated from atmospheric sources in both catchments only during the first days of melt. In the undisturbed catchment, low NO_3^- concentrations and elevated streamwater $\delta^{18}O\text{-}NO_3^-$ values relative to the disturbed catchment indicate that NO_3^- export was suppressed by sink mechanisms. In contrast, low $\delta^{18}O\text{-}NO_3^-$ values and high NO_3^- concentrations in runoff from the disturbed catchment indicate that the supply of NO_3^- from microbial sources far outweighed sinks in the watershed. This research demonstrates that ALDs enhanced the export of microbially derived NO_3^- relative to undisturbed watersheds, and that this is likely a result of limited NO_3^- retention and enhanced nitrification in the mineral soils exposed in the scar zones of ALDs.

Keywords Active layer detachments · Atmospheric deposition · Denitrification · High Arctic · Nitrate · Nitrification

Responsible Editor: W. Troy Baisden.

N. L. Louiseize (✉) · M. J. Lafrenière
Department of Geography, Queen's University, Kingston, ON K7L 3N6, Canada
e-mail: nlouiseize@gmail.com

M. J. Lafrenière
e-mail: melissa.lafreniere@queensu.ca

M. G. Hastings
Department of Geological Sciences, Brown University, Providence, RI 02912, USA
e-mail: meredith_hastings@brown.edu

Introduction

Recent studies show that permafrost degradation may disrupt nitrogen (N) transport dynamics and lead to greater watershed nitrate (NO_3^-) export due to increases in streamwater NO_3^- concentrations (Bowden et al. 2008; Harms et al. 2014; Louiseize and Lafrenière 2013). For example, Bowden et al. (2008) reported that NO_3^- concentrations immediately downstream of thermokarst gullies and thaw slumps were exceptionally high compared to concentrations upstream of these features. Similar results were documented by Louiseize and Lafrenière (submitted), who show that

permafrost disturbances resulted in significantly higher NO_3^- concentrations and therefore much larger seasonal fluxes of NO_3^- compared to undisturbed watersheds. This is of concern because even minor changes in N export can impact downstream aquatic ecosystem function (McClelland et al. 2007).

Despite the mounting evidence that various types of permafrost disturbance enhance NO_3^- concentrations in Arctic rivers (Bowden et al. 2008; Frey and McClelland 2009; Harms and Jones 2012; Harms et al. 2014; Louiseize and Lafrenière submitted), very little is known about the impact of permafrost disturbances on the sources and processes that regulate seasonal NO_3^- concentrations in High Arctic streams. Active layer detachments (ALDs) are landslide type slope disturbances that cause the vegetation cover and thawed soils to move downslope along the ice-rich permafrost, thus leading to the exposure of mineral soils in the scar zone as well as amassment of soils at the base of slopes (Lewkowicz and Harris 2005). Hence, ALDs represent a type of permafrost disturbance that can affect hydrologic pathways and response, which are among the main controls of dissolved inorganic N (DIN, including ammonium (NH_4^+) and NO_3^-) concentrations in streams (Petrone et al. 2006; Cooper et al. 2007). The ensuing changes to subsurface environmental conditions, such as soil temperature, moisture, oxygen availability, and nutrient content, may also stimulate microbial activity (Paulter et al. 2010) and alter the relative importance of productive (e.g., nitrification) and consumptive N cycling processes (e.g., denitrification, vegetative and microbial uptake) in disturbed areas (Harms et al. 2014). ALDs could therefore mobilize relatively older or deeper sources of N that were previously isolated from cycling activities and hydrologic export, as hypothesized for permafrost disturbances in general (Shaver et al. 1992; Levine and Whalen 2001; Jones et al. 2005; McClelland et al. 2007; Frey and McClelland 2009; Woods et al. 2011; Keuper et al. 2012; Harms and Jones 2012; Harms et al. 2014). The occurrence of ALDs and other types of disturbance is expected to increase with regional climate warming (Lamoureux and Lafrenière 2009; Vincent et al. 2013); hence, it is important to understand how these disturbances affect watershed N dynamics and stream NO_3^- concentrations.

The aim of this research is to investigate how ALDs influence the processes that control streamwater NO_3^- concentrations in High Arctic watersheds. We approached this question by comparing the seasonal evolution of the stable isotope compositions of species of NO_3^-, including nitrogen in nitrate (δ^{15}N-NO_3^-) and oxygen in nitrate (δ^{18}O-NO_3^-), as well as major ion chemistry in precipitation and runoff from two small headwater catchments, one that is undisturbed and one that has recently been affected by ALDs, at the Cape Bounty Arctic Watershed Observatory (CBAWO) on Melville Island, Nunavut, Canada (Fig. 1). These data are supplemented by measurements of precipitation and stream discharge. To our knowledge, this is the first study that uses stable isotopes of NO_3^- to investigate the seasonality and sources of NO_3^- in runoff from a disturbed catchment in a continuous permafrost watershed. This is an important step towards understanding how disturbances such as ALDs affect fluvial N export and catchment N dynamics in an understudied region that is experiencing significant environmental change.

Methods

Study site

This study was conducted in two small hillslope catchments within the West watershed at the Cape Bounty Arctic Watershed Observatory (74°54′N, 109°35′W) on Melville Island, Nunavut (Fig. 1). Continuous permafrost underlies the study area and active layer depths in hill slopes are typically between 0.60 and 1 m during the peak growing season. Vegetation communities in the catchments vary according to moisture conditions (Atkinson and Treitz 2012). Low moisture areas host polar desert communities such as *Thamnolia subliformis* spp. (Worm Lichen) and *Cetraria nivalis* spp. (Snow lichen) but primarily consist of rock or till. Areas with moderately wet soils are predominantly colonized by mesic heath type vegetation such as *Nostoc commune* spp. (nitrogen fixing cyanobacteria) and *Salix arctica* spp., while areas that remain thoroughly saturated throughout the growing season are totally vegetated with wet sedge community type, including *Eriophorium* spp. and *Sphagnum* spp. (Atkinson and Treitz 2012).

The disturbed Ptarmigan (PT, unofficial name) catchment encompasses an area of 213,000 m^2 and

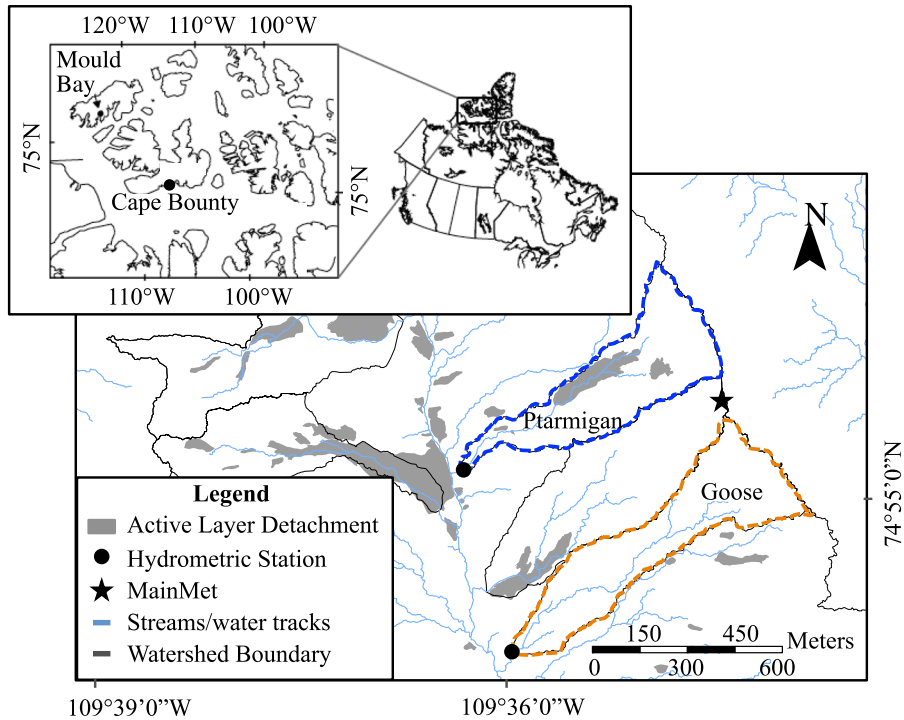

Fig. 1 Map illustrating the location of Cape Bounty (*inset*), MainMet, and the hydrometric stations of the Ptarmigan (*blue*) and Goose (*orange*) catchments. (Color figure online)

contains three disturbances that formed in late July 2007. These slides were triggered by a significant rainfall event that followed an extended period of unusually warm temperatures (Lamoureux and Lafrenière 2009). Collectively, the ALDs occupy approximately 12 % of the total catchment area (Lafrenière and Lamoureux 2013). These include an isolated, compact ALD (3,774 m^2), which was actively retrogressing during the field season, and two elongate ALDs (19,587 and 676 m^2) (Ashley Rudy, unpublished data), whose scar zones expose the underlying mineral soils and remain completely free of vegetation. In undisturbed areas of the catchment, the dominant vegetation classes are mesic heath and polar semi-desert. The stream draining PT is well-incised in the mineral soils along most of its length, and flows through the length of the two elongate disturbances. Due to the stream's linkage to these disturbances, the water exported from PT provides a good representation of the potential impacts of ALDs on water quality and on biogeochemical processes occurring within disturbed soils. The reference catchment, Goose (GS, unofficial name), covers an area of 179,000 m^2 and remains completely free of any physical disturbances. The catchment is drained by a poorly incised, vegetated channel or water track. Although GS is the smaller catchment, its topography allows for greater snow accumulation and thus an extended runoff period compared to PT. The dominant vegetation communities in this catchment are mesic heath and wet sedge.

The snowmelt season typically lasts from early to mid-June until mid-July, when river discharge is primarily sustained by snowmelt from the thick snow packs in channels and depressions. Beyond early or mid July, hill slope streams typically dry up, and flow only resumes following rainfall (Lafrenière and Lamoureux 2013). Rainfall events are typically infrequent and of low magnitude (Lafrenière and Lamoureux 2008), but mean precipitation amounts in the summer have ranged between 2.5 and 66.8 mm from 2003 to 2012 (Favaro and Lamoureux submitted).

Hydrological and environmental measurements

Instantaneous discharge was obtained by converting measurements of stage taken within 8" cutthroat

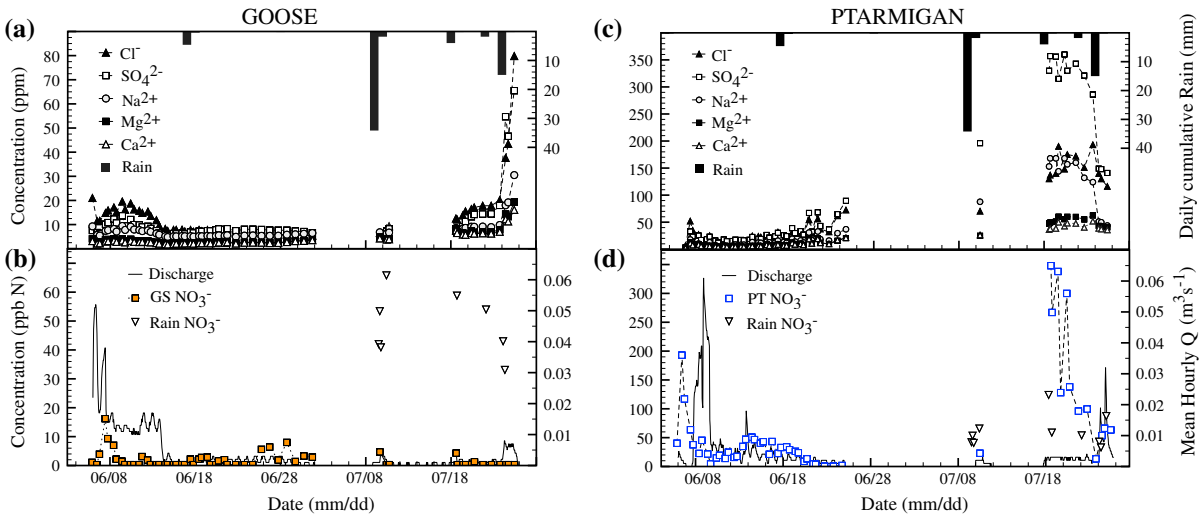

Fig. 2 **a** Dissolved ion concentrations in Goose and daily cumulative rainfall. **b** NO_3^- concentrations and mean hourly discharge in Goose. **c** Dissolved ion concentrations in Ptarmigan and daily cumulative rainfall. **d** NO_3^- concentration and mean hourly discharge in Ptarmigan. Note the differences in scale for NO_3^- and major ion concentrations between Goose and Ptarmigan

flumes at the outlet of each catchment using standard equations for the flumes (American Society of Civil Engineers 1974). Stage was recorded every 10 min using Onset U20 level loggers (±2 mm) that were adjusted for barometric pressure using a second U30 logger installed at Main Met (Fig. 1). Instantaneous discharge was converted to average hourly discharge (Q; $m^3\ s^{-1}$) so as to smooth out the hydrograph. In-situ water temperature (±1 °C), pH (±0.1 pH), and electrical conductivity (±2 % µS cm^{-1}) were measured during stream sampling with an Extech Exstik II pH/conductivity meter. Shielded air temperature was recorded at Main Met 1.5 m above ground using an Onset Temperature/RH smart sensor (±0.21 °C temperature, ±2.5 % relative humidity) and precipitation was measured with an Onset industrial tipping bucket gauge (0.2 mm).

Hydrologic regimes

Seasonal hydrographs for PT and GS were divided into nival melt, baseflow, and stormflow seasons according to seasonal changes in discharge and the occurrence of rainfall. The nival melt period was determined to commence on June 5 and transitioned into baseflow on June 16, which lasted until the end of streamflow on June 24 in PT and July 1 in GS. The stormflow period encompasses two series of runoff-generating precipitation events that rejuvenated discharge in both streams from July 9–10 and from July 18–25 (Fig. 2b, d).

Sample collection

Stream water sampling began on the first day of flow (June 5, 2012) and continued until the end of baseflow (June 24 in PT and July 1 in GS) and during stormflow (July 9–10; July 18–25). Samples were collected at stream outlets twice daily at approximately 10:00 and 18:00, near the times of minimum and maximum discharge, respectively, during the nival melt and stormflow periods, and once daily at approximately 18:00 during baseflow. Samples were collected using 1 L Nalgene bottles, which were tripled-rinsed with distilled water prior to deployment and with streamwater immediately before sampling. The bottles were completely filled and were kept cool and in the dark until filtration (typically within 30–120 min).

Precipitation samples were collected using passive rainfall samplers. These consisted of 20 L polycarbonate funnels (24 cm diameter) that were secured within a PVC frame so that the openings were elevated 50 cm above ground. The funnel drained into a removable 45 mL amber EPA vial by means of 10 cm long Tygon R-3603 tubing, which passed through the Teflon septum of the vial. The EPA vial

was suspended within a removable 1 L Nalgene bottle that was secured to the collector and covered with black out material so as to protect the collection vial from UV light. In order to exclude dry deposition, the funnels were covered with plastic lids at all times except during precipitation events, when the covers were manually removed. Upon sample retrieval, the EPA vials were removed from the collectors, sealed with new caps, and replaced with a clean vial. All vials and caps were triple rinsed with distilled water before and after use.

All samples for dissolved ion analysis (including dissolved inorganic N (DIN)) were syringe filtered through 0.22 μm PVDF membrane filters. Syringes were triple-rinsed with distilled water before and after use, and new filters were used for each sample. All filters were rinsed with 10 mL of sample that was discarded before filling the vials. Samples were stored in HDPE vials or bottles that were pre-cleaned (triple soaked and rinsed with Milli-Q water at Queen's University), rinsed with filtered sample, and filled with no headspace. Aliquots for dissolved ion analysis were refrigerated until analyzed at Queen's University, while samples for stable isotope analyses ($^{15}N/^{14}N$ and $^{18}O/^{16}O$ of NO_3^-) were frozen in the field and during shipment, and thawed immediately prior to analysis at Brown University.

Stream samples that were collected for TDN and dissolved organic carbon (DOC) analyses were filtered through pre-combusted 0.7 μm glass fiber filters (GF/F) with a glass filtration apparatus. The filtration apparatus was triple-rinsed with distilled water before use as well as between samples and soaked in 3 % hydrochloric acid every night. TDN and DOC samples were acidified to pH 2 and kept in 45 ml amber EPA vials with Teflon lined septa that were rinsed with filtered sample and filled to eliminate headspace. Samples were refrigerated and kept in the dark until analyzed at Queen's University.

Analytical methods

Major ions and N species

Dissolved inorganic anions (Cl^-, SO_4^{2-}, NO_2^-, NO_3^-) and cations (K^+, Na^+, Ca^{2+}, and Mg^{2+}) were quantified simultaneously by liquid ion chromatography with a Dionex ICS-3000. Anions were measured using KOH eluent with a gradient elution of 11–40 mM KOH flowing at 1.0 ml min^{-1} through an AS18 analytical column and an ASRS 300 suppressor. Cations were quantified isocratically using 16 mM methane sulphonic acid eluent flowing at 0.5 ml min^{-1} through a CS12A-5 analytical column and a CSRS 300 suppressor. Detection limits were calculated as three times the standard deviation of replicates of the low level standards, and were <0.005 ppm except for Mg^{2+} (0.016 ppm) and Ca^{2+} (0.039 ppm). Nonetheless, the concentrations of these species in the samples were at least 100 times higher than these background levels. The analytical uncertainty for most ion analyses, determined by the mean standard error of replicate samples, was better than 2 %. For NO_3^-, the analytical uncertainty was 2 % and the detection limit was 0.003 ppm (or 0.7 ppb N). For NO_2^-, the analytical error was 2.5 % and the detection limit was 0.01 ppb (or 0.03 ppb N); however NO_2^- in most samples was below detection limit.

Concentrations of NH_4^+ were measured by colorimetry using an Astoria Pacific FASPac II Flow Analyser. The detection limit was <0.01 ppm N and the analytical error was 0.9 %. DIN was calculated as the sum of the N mass from NH_4^+, NO_3^- and NO_2^- (when detectable).

Samples of DOC and TDN were analyzed simultaneously by high temperature combustion and NDIR and chemiluminescent detection using a Shimadzu TOC-VPCH/TNM equipped with a high sensitivity catalyst system. Analytical errors for DOC and TDN were 2.9 and 2.3 %, respectively based on replicate analyses of standards. Detection limits were 0.080 ppm for DOC and 0.015 ppm N for TDN. DON was determined as the difference between TDN and DIN.

Stable isotope ratios

The stable isotope ratio of oxygen in water (H_2O; $^{18}O/^{16}O$) was measured using a Los Gatos Research Liquid–Water Isotope Analyzer, which vaporizes injected sample and measures its absorbance relative to Vienna Standard Mean Ocean (VSMOW). All sample runs include replicate analyses of standards produced by Los Gatos (e.g., LGR1A, $\delta^{18}O = -19.5$ ‰ and $\delta D = -154.3$ ‰; LGR3A, $\delta^{18}O = -13.1$ ‰ and $\delta D = -96.4$ ‰), and samples are

corrected to their values. Reproducibility (1σ) based on repeated measurements of standards is ±0.25 ‰ for $\delta^{18}O$. The standard deviation for replicate analyses of samples in this dataset was 0.05 ‰ for $\delta^{18}O$.

Stable isotope ratios of species of NO_3^- ($^{15}N/^{14}N$ and $^{18}O/^{16}O$) were quantified using the denitrifier method at Brown University and standardized based on N_2 in air and VSMOW, respectively. This technique employs denitrifying bacteria that lack N_2O-reductase in order to transform as little as 5–10 nmol of NO_3^- in water samples to N_2O, the latter of which is then analyzed for stable isotope composition by an isotope ratio mass spectrometer in continuous flow mode (Sigman et al. 2001; Casciotti et al. 2002). All sample runs include replicate analyses of NO_3^- standards USGS34, USGS35, and IAEA-N3, and sample values are corrected to the internationally recognized values for $\delta^{15}N$ (USGS34 (−1.8 ‰); IAEA-N3 (+4.7 ‰)) and $\delta^{18}O$ (USGS34 (−27.9 ‰), USGS35 (+57.5 ‰), IAEA-N3 (+25.6 ‰)) (Böhlke et al. 2003) based on the framework presented in Kaiser et al. (2007). Typical reproducibility (1σ) based on repeated measurements of isotopic standards is ±0.2 ‰ for $\delta^{15}N$ and ±0.6 ‰ for $\delta^{18}O$. The paired standard deviation for replicate analyses of samples in this dataset was 0.1 and 0.5 ‰ for $\delta^{15}N$ and $\delta^{18}O$, respectively. The majority of samples were run with 10 nmol of NO_3^-, however, if sample volume or concentration was limited, analyses were completed with only 5 nmol of NO_3^-.

Statistical analyses

Pearson's correlation analyses were applied in order to determine relationships between NO_3^- and other dissolved organic and inorganic ions (e.g., DON, DOC, NH_4^+, Cl^-, SO_4^{2-}, K^+, Na^+, Mg^{2+}, and Ca^{2+}) for the nival, baseflow, and stormflow periods in PT and GS. All analyses were performed in StatPlus using a significance level of $\alpha = 0.02$.

Results

Hydrology

Seasonal discharge varied somewhat between catchments. Discharge commenced on June 5 in both streams, and peak snowmelt discharge occured on June 6 in GS and June 8 in PT (Fig. 2b, d). Streamflow decreased considerably after June 15 in both catchments and ceased in PT on June 24, while residual snow packs and wetter soils in GS sustained baseflow until July 1. Discharge was rejuvenated from July 9–10 in both streams due to a hydrologically significant rainfall event (Fig. 2b, d); however, dry antecedent moisture conditions muted the hydrograph responses. Due to wetter antecedent moisture conditions, subsequent smaller magnitude rainfall events regenerated and sustained discharge in both catchments from July 18 to July 25, and permitted the mean hourly discharge to reach 0.03 $m^3\ s^{-1}$ in PT and 0.007 $m^3\ s^{-1}$GS on July 24 (Fig. 2b, d).

Dissolved ion chemistry and N species composition

In GS, all dissolved ions except for NO_3^- followed similar trends and NO_3^- concentrations were generally low throughout the season (Fig. 2a, b). NO_3^- in GS was near detection limit at the onset of melt and peaked at 16.2 ppb N on June 7 concomitant with the second peak in snowmelt runoff (Fig. 2b). NO_3^- decreased to below detection limit (BDL) as discharge declined on June 9, where as major ions (Cl^-, SO_4^{2-}, Na^+, Mg^{2+}, and Ca^{2+}) reached their peak concentrations of the nival melt period at this time. Hence, NO_3^- concentrations during the nival melt (June 5–15) in GS were not significantly correlated with any ion (Table 1). The mean NO_3^- concentration during nival melt in GS was 2.4 ± 4.0 ppb N and that during baseflow was 2.1 ± 2.2 ppb N (Table 2).

During stormflow, NO_3^- in GS runoff was mostly BDL even though rainfall NO_3^- concentrations were as high as 124 ppb N. All ion concentrations (except NO_3^-) increased dramatically with discharge on July 24 and reached their seasonal highs on July 25. No significant correlations existed between NO_3^- and other dissolved ions during stormflow (Table 1). The mean stormflow NO_3^- concentration (for all events from July 9 to 25) was 0.90 ± 1.5 ppb N (Table 2).

In PT, NO_3^- and major ion concentrations greatly exceeded those of GS and trends of NO_3^- closely followed those of major ion concentrations except during baseflow (June 16–24). NO_3^- concentrations during the nival melt were significantly correlated

Table 1 Correlation of NO_3^- with major ions, NO_2^-, NH_4^+, DON and DOC for Goose and Ptarmigan during the nival, baseflow, and stormflow periods

	GS NIVAL ($n = 21$)										PT NIVAL MELT ($n = 21$)								
	Cl^-	SO_4^{2-}	Na^+	K^+	Mg^{2+}	Ca^{2+}	NO_3^-	NO_2^-	NH_4^+	DOC	Cl^-	SO_4^{2-}	Na^+	K^+	Mg^{2+}	Ca^{2+}	NO_2^-	NH_4^+	DOC
NO_3^-	0.23	0.36	0.20	0.27	0.46	0.41	1.0				***0.93***	***0.67***	***0.72***	***0.95***	***0.85***	***0.78***	1.0		
NO_2^-	−0.01	0.03	−0.02	0.05	0.11	0.12	0.50	1.0			–	–	–	–	–	–	–	–	–
NH_4^+	**0.57**	0.11	0.50	***0.95***	**0.56**	0.45	0.25	0.18	1.0		0.16	0.18	0.16	0.2	0.26	0.26	0.2	1.0	
DOC	0.46	−0.01	0.36	***0.99***	0.48	0.34	0.26	0.05	***0.94***	1.0	**0.60**	0.28	0.23	***0.85***	**0.57**	0.50	***0.81***	0.15	1.0
DON	0.28	−0.14	0.20	***0.88***	0.31	0.18	0.12	0.00	***0.83***	***0.89***	***0.67***	0.42	0.41	***0.82***	***0.67***	**0.61**	***0.83***	0.05	***0.89***
	GS BASEFLOW ($n = 23$)										PT BASEFLOW ($n = 15$)								
	Cl^-	SO_4^{2-}	Na^+	K^+	Mg^{2+}	Ca^{2+}	NO_3^-	NO_2^-	NH_4^+	DOC	Cl^-	SO_4^{2-}	Na^+	K^+	Mg^{2+}	Ca^{2+}	NO_2^-	NH_4^+	DOC
NO_3^-	−0.39	−0.04	0.39	−0.15	0.32	0.38	1.0				**−0.65**	**−0.67**	**−0.63**	−0.59	**−0.62**	**−0.66**	1.0		
NO_2^-	**0.59**	−0.15	−0.23	0.42	−0.13	−0.18	0.00	1.0			–	–	–	–	–	–	–	–	–
NH_4^+	***−0.65***	−0.13	**0.63**	−0.36	0.47	**0.55**	***0.67***	−0.4	1.0		0.03	0.04	0.01	−0.08	0.09	0.06	−0.12	1.0	
DOC	−0.39	**−0.6**	***0.83***	−0.05	***0.91***	***0.89***	0.35	−0.17	0.38	1.0	−0.18	−0.16	−0.04	−0.07	−0.05	−0.10	0.19	−0.23	1.0
DON	−0.23	***−0.71***	***0.76***	0.10	***0.86***	***0.82***	0.17	−0.06	0.19	***0.95***	−0.32	−0.25	−0.20	−0.18	−0.26	−0.28	0.22	−0.58	**0.61**
	GS STORMFLOW ($n = 14$)										PT STORMFLOW ($n = 13$)								
	Cl^-	SO_4^{2-}	Na^+	K^+	Mg^{2+}	Ca^{2+}	NO_3^-	NO_2^-	NH_4^+	DOC	Cl^-	SO_4^{2-}	Na^+	K^+	Mg^{2+}	Ca^{2+}	NO_2^-	NH_4^+	DOC
NO_3^-	−0.19	−0.23	−0.16	0.04	−0.05	−0.03	1.0				−0.01	**0.66**	**0.67**	0.44	0.19	−0.07	1.0		
NO_2^-	0.02	0.15	0.06	−0.08	0.13	0.13	−0.32	1.0			–	–	–	–	–	–	–	–	–
NH_4^+	0.00	0.03	0.04	0.06	0.11	0.12	0.36	−0.29	1.0		0.50	0.21	0.24	0.40	0.44	0.52	−0.03	1.0	
DOC	−0.52	−0.57	−0.49	−0.34	−0.52	−0.52	0.39	−0.21	0.22	1.0	−0.43	***−0.83***	***−0.84***	***−0.77***	−0.60	−0.47	−0.50	−0.35	1.0
DON	−0.54	**−0.64**	−0.51	−0.31	−0.48	−0.47	0.45	−0.02	0.23	***0.87***	−0.12	−0.48	−0.51	−0.40	−0.28	−0.14	−0.61	−0.35	0.61

Bold and italicized text indicates a significance level of $p < 0.001$, and bold text indicates $p < 0.02$

Table 2 Mean concentrations of NO_3^- and major ions for rain and throughout the season during the nival, baseflow, and stormflow periods in Goose and Ptarmigan

Mean concentrations							
	$N\text{-}NO_3^-$ (ppb)	Cl^- (ppm)	SO_4^{2-} (ppm)	Na^+ (ppm)	K^+ (ppm)	Mg^{2+} (ppm)	Ca^{2+} (ppm)
GS							
Nival melt	2.4 ± 4.0	14 ± 4.0	8.8 ± 2.3	7.0 ± 1.4	1.4 ± 1.4	3.1 ± 0.67	2.6 ± 0.50
Baseflow	2.1 ± 2.2	6.8 ± 0.86	7.4 ± 0.60	5.4 ± 0.38	0.29 ± 0.08	2.7 ± 0.36	2.5 ± 0.38
Stormflow	0.90 ± 1.5	22 ± 19	20 ± 19	11 ± 6.5	0.24 ± 0.12	8.2 ± 4.2	7.3 ± 3.4
Seasonal	1.9 ± 2.8	13 ± 11	11 ± 11	7.5 ± 4.1	0.68 ± 1.0	4.3 ± 3.2	3.8 ± 2.7
PT							
Nival	44 ± 42	20 ± 9.6	19 ± 5.9	9.6 ± 3.5	1.3 ± 0.6	6.3 ± 2.2	5.8 ± 1.9
Baseflow	18 ± 14	37 ± 16	42 ± 20	20 ± 8.4	1.5 ± 0.4	12 ± 4.8	12 ± 4.9
Stormflow	149 ± 121	145 ± 33	279 ± 87	124 ± 48	4.4 ± 1.0	50 ± 11	41 ± 7.1
Seasonal	64 ± 85	59 ± 57	95 ± 121	43 ± 55	2.2 ± 1.5	20 ± 20	17 ± 15
Rain	60 ± 27	0.17 ± 0.12	0.19 ± 0.10	0.11 ± 0.07	0.05 ± 0.04	0.02 ± 0.02	0.07 ± 0.04

"±" refers to 1 standard deviation from the mean

with DON, DOC, and all major ions (Table 1). The peak melt NO_3^- concentration in PT occurred on the second day of melt and measured 193 ppb N, thereby exceeding the peak NO_3^- concentration in GS by a factor of twelve. NO_3^- concentrations in PT decreased to 4.3 ppb N by June 9, but higher concentrations (15–51 ppb N) were sustained from June 10 to June 20 before gradually decreasing to near detection limit until the end of streamflow (June 24). During the nival melt, the mean NO_3^- concentration was 44 ± 42 ppb N. The mean NO_3^- concentration during baseflow was 18 ± 14 ppb N.

Stormflow runoff produced the highest measured solute concentrations in PT. On July 18, shortly after rainfall runoff recommenced, NO_3^- reached a seasonal high of 348 ppb N, thus exceeding the highest recorded rainfall NO_3^- concentration by 224 ppb N. Streamwater NO_3^- in PT measured above 128 ppb N until July 20. NO_3^- in PT during stormflow was significantly positively correlated with Na^+ and SO_4^2 and had strong negative relationships with DON and DOC (Table 1). The dominant ion during stormflow was SO_4^{2-} (279 ± 87 ppm) and the mean stormflow NO_3^- concentration was 149 ± 121 ppb N.

Stable isotopes of NO_3^-

Although samples for stable isotopes of NO_3^- were collected throughout the entire sampling campaign, only a subset of samples was selected for analysis based on notable changes in discharge and NO_3^- concentration. Note that NO_3^- concentrations in GS were often below the analytical requirement (5–10 nmol), hence there are fewer data points for GS relative to PT.

$\delta^{15}N\text{-}NO_3^-$

The seasonal $\delta^{15}N$ values of streamwater NO_3^- were on average higher in PT (+4.1 ‰, $n = 15$) than in GS (+1.6 ‰, $n = 11$) and ranged from −7.1 to +15.8 ‰ in PT and from −7.9 to +13.6 ‰ in GS (Fig. 3a). Values of $\delta^{15}N\text{-}NO_3^-$ were negative during the initial days of streamflow in both catchments (from −7.1 to −2.6 ‰ in PT and −7.3 to −4.1 ‰ in GS from June 5 to 7) and increased towards positive values after June 7. The $\delta^{15}N\text{-}NO_3^-$ values in both streams were exceptionally high near the end of baseflow, peaking at +15.8 ‰ in PT on June 24 and reaching +12.3 ‰ on June 26 in GS (Fig. 3a). The seasonal peak $\delta^{15}N\text{-}NO_3^-$ value in GS (+13.6 ‰) occurred at the onset of the second stormflow runoff event on July 18.

Rainwater $\delta^{15}N\text{-}NO_3^-$ values generally remained between +0.1 and +2.0 ‰ (mean = +1.0 ‰ ± 1.0, $n = 7$), thus measuring several permil lower than stormflow runoff values. The highest rainfall $\delta^{15}N$ value measured +2.7 ‰ and was collected on July 24 at 2:30 am (Fig. 3a).

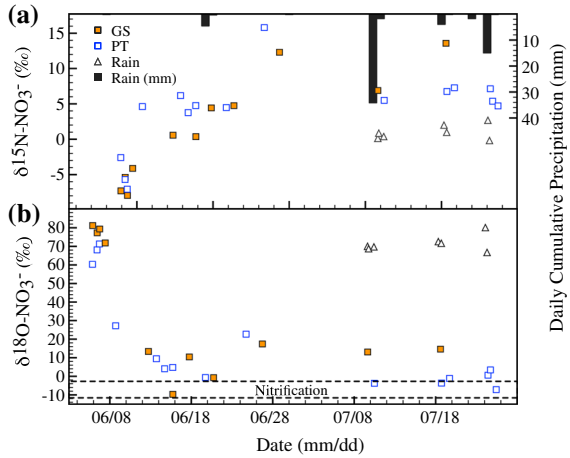

Fig. 3 **a** Daily cumulative rainfall amount and values of δ^{15}N-NO_3^- in rainfall and streamwater from Goose and Ptarmigan. **b** Values of δ^{18}O-NO_3^- in rainfall and stream water from Goose and Ptarmigan. The *black dashed box* represents the expected range of δ^{18}O-NO_3^- values of NO_3^- produced from nitrification (−10.6 to −2.2 ‰)

$\delta^{18}O$-NO_3^-

Values of δ^{18}O-NO_3^- were highly enriched during the beginning of streamflow (June 5–7) in both catchments compared to the rest of the season (Fig. 3b). During the first 3 days of sampling, δ^{18}O-NO_3^- ranged from + 60.3 to + 71.3 ‰ (mean = 66.6 ‰ ± 5.7, $n = 3$) in PT and from +71.9 to +81.2 ‰ (mean = 77.4 ‰ ± 5.7, $n = 4$) in GS. The δ^{18}O-NO_3^- values in PT dropped to +27.2 ‰ on June 8 and remained below +9.5 ‰ after June 13 except on the last day of baseflow (June 24) when δ^{18}O reached +22.7 ‰. The δ^{18}O-NO_3^- values in GS were typically higher than those of PT after June 12, but did fall to −9.7 ‰ on June 15 and −0.7 ‰ on June 20.

During stormflow, δ^{18}O-NO_3^- values in PT plotted between −7.2 and +3.4 ‰, and those in GS measured +13.1 and +14.6 ‰. The δ^{18}O-NO_3^- values of rainwater NO_3^- varied between +66.7 and +80.1 ‰ (mean = +71.4 ‰ ± 4.3).

Discussion

Constraining sources of NO_3^-

In unpolluted watersheds, NO_3^- in runoff predominantly originates from atmospheric (NO_3^- in snow or rain) or microbial (NO_3^- mineralized from soil or dissolved organic matter (SOM, DOM) or nitrified from NH_4^+) sources. Streamwater δ^{18}O-NO_3^- values can be used to determine the relative contributions of these two sources to NO_3^- in runoff because atmospheric and microbial processes impart δ^{18}O-NO_3^- values that are readily distinguishable from one another (Kendall et al. 2007). Atmospheric NO_3^- is characterized by high δ^{18}O values due to the signature imparted by ozone (O_3) ($\sim$100 ‰) during formation of nitrogen oxides (NO_x) in the atmosphere (Hastings et al. 2003). Hence, high streamwater δ^{18}O-NO_3^- values (>+60 ‰) indicate inputs primarily from atmospheric deposition (Kendall et al. 2007). Much lower streamwater δ^{18}O-NO_3^- values (−10 to +10 ‰ with δ^{18}O-H_2O values between −25 and +4 ‰) point towards microbial contributions because of the relatively low stable isotope values for oxygen in the water (H_2O) and air (O_2) involved in nitrification, a process whereby NH_4^+ is oxidized to NO_3^- under aerobic conditions (e.g., $NH_4^+ \rightarrow NO_2^- \rightarrow NO_3^-$) (Kendall et al. 2007). Studies of nitrification have shown that atmospheric O_2 and H_2O typically provide 1/3 and 2/3, respectively, of the oxygen atoms in nitrified NO_3^- (Kendall 1998). Using this relationship, the range of potential streamwater δ^{18}O-NO_3^- values derived from microbial nitrification(δ^{18}O-$NO_{3\ \text{nitrification}}^-$) can be calculated by employing the following equation:

$$\delta^{18}\text{O} - \text{NO}_{3\ \text{nitrification}}^- = 0.33 * \delta^{18}\text{O} - \text{O}_2 + 0.67 * \delta^{18}\text{O} - \text{H}_2\text{O}, \quad (1)$$

where δ^{18}O-O_2 represents the stable isotope composition of atmospheric O_2 (which is assumed to be +23.5 ‰, Kendall et al. 2007) and δ^{18}O-H_2O is the isotope composition of the streamwater collected. Using streamwater δ^{18}O-H_2O values from this study (−27.4 to −14.9 ‰, Table 3), Eq. 1 yields a range of δ^{18}O-$NO_{3\ \text{nitrification}}^-$ values between −10.6 and −2.2 ‰. Although more recent laboratory studies suggest that there may be a greater dependence on the ^{18}O in H_2O used during nitrification (Buchwald and Casciotti 2010; Snider et al. 2010), the data in this study are well captured by the range predicted by the 1/3 and 2/3 relationship. Note that δ^{18}O-$NO_{3\ \text{nitrification}}^-$ values can exceed this hypothetical range, as processes occurring within natural systems may violate the assumptions inherent to Eq. 1. Processes that could

Table 3 Dates and $\delta^{18}O$-H_2O values of stream water samples used for mixing model analysis

Ptarmigan	$\delta^{18}O$-H_2O	Goose	$\delta^{18}O$-H_2O
06-05 21:00	−26.5	06-05 21:35	−25.2
06-06 10:40	−27.3	06-06 11:00	−23.5
06-06 17:37	−27.4	06-06 18:20	−24.5
06-08 17:20	−25.6	06-07 10:35	−22.8
06-13 17:25	−22.6	06-12 17:54	−24.9
06-14 17:31	−22.8	06-15 17:52	−24.8
06-15 17:35	−21.7	06-17 18:22	−24.1
06-19 17:52	−20.2	06-20 17:53	−22.6
06-24 17:33	−17.1	06-26 17:32	−21.1
07-10 11:35	−17.0	07-09 15:40	−17.2
07-18 17:21	−17.5	07-18 14:17	−14.9
07-19 16:54	−17.0		
07-24 10:05	−16.2		
07-24 17:16	−16.0		
07-25 10:25	−16.2		

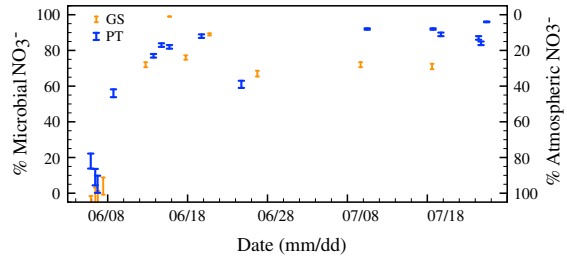

Fig. 4 Results of mixing model showing the approximate range of the fraction of stream water NO_3^- derived from atmospheric deposition (F_{precip}) and microbial NO_3^- in Goose and Ptarmigan using mean (71.4 ‰) and maximum (80.1 ‰) $\delta^{18}O$-$NO_{3precip}^-$ values found in rainfall at Cape Bounty and the calculated minimum (−10.6 ‰) for the $\delta^{18}O_{nitrification}$ end-member value

yield higher than expected values of $\delta^{18}O$-$NO_{3\ nitrification}^-$ include: a higher fraction of O atoms derived from atmospheric O_2 and H_2O (Aravena et al. 1993); evaporative enrichment of the source water $\delta^{18}O$ (Böhlke et al. 1997) and; incorporation of O_2 which has become enriched relative to the assumed atmospheric value due to high rates of respiration in soils or sediments (Kendall 1998).

Since streamwater $\delta^{18}O$-NO_3^- values typically lie between the values expected for atmospheric NO_3^- and microbially derived (nitrified) NO_3^-, the relative contributions of atmospheric NO_3^- and nitrified-NO_3^- to streamwater NO_3^- were estimated by employing a two end-member mixing model (Kendall 1998; Barnes et al. 2008):

$$\left(\delta^{18}O_{stream} - \delta^{18}Onitrification\right)/\left(\delta^{18}O_{precip} - \delta^{18}Onitrification\right) = F_{precip}, \quad (2)$$

where $\delta^{18}O_{stream}$, $\delta^{18}O_{precip}$, and $\delta^{18}O_{nitrification}$ represent the $\delta^{18}O$-NO_3^- values of the collected streamwater, rainfall, and the calculated minimum nitrification value (−10.6 ‰), respectively. Hence, F_{precip} is the approximate fraction of streamwater NO_3^- derived purely from atmospheric NO_3^- (Fig. 4). Since rainfall $\delta^{18}O$-NO_3^- varied throughout the season, we estimated a range of F_{precip} by using the mean and maximum $\delta^{18}O$-NO_3^- values found in the rain.

While this model can help apportion NO_3^- between these two end member sources, the co-occurrence of other cycling processes such as assimilation or denitrification and their consequent fractionations on $\delta^{18}O$ may confound the results (Kendall et al. 2007). For instance, the relative contribution of nitrified-NO_3^- may appear diminished while that of atmospheric NO_3^- may appear higher if denitrification and/or assimilation are occurring, as these processes both cause the $\delta^{18}O$ value of the residual NO_3^- pool to increase (Kendall et al. 2007). The $\delta^{18}O$-NO_3^- values and mixing model results on June 24 in PT and June 26 in GS provide a good example of this (Figs. 3a, b, 4). The increases in $\delta^{18}O$-NO_3^- in PT on June 24 and in GS on June 26 relative to the previous samples suggest that the fraction of streamwater NO_3^- derived from atmospheric deposition increased by approximately 27 % in PT and 21 % in GS compared to the previous samples. However, since there was no rainfall during that interval, it is unlikely that there was an increase in the NO_3^- contributed from atmospheric deposition. Instead, what appears to be a greater contribution from atmospheric sources on June 24 in PT and June 26 in GS is actually more likely the result of consumptive processes (denitrification and assimilation) generating higher $\delta^{18}O$-NO_3^- and $\delta^{18}N$ values and relatively lower NO_3^- concentrations (Fig. 5). Hence, the results of this mixing model must be interpreted with the potential impact of these processes in mind.

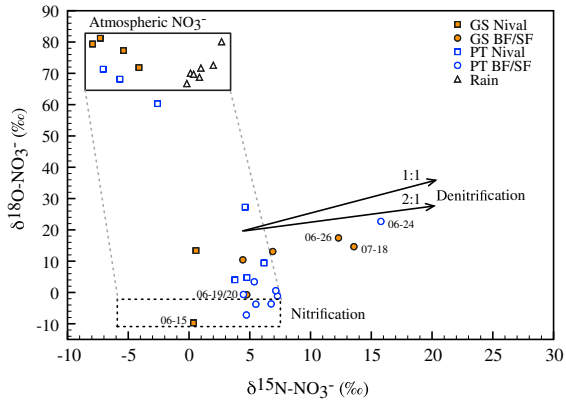

Fig. 5 Rainwater NO_3^- and sources of stream water NO_3^- in Goose and Ptarmigan for select samples collected during the nival melt, baseflow, and stormflow periods. The larger *black rectangle* denotes $\delta^{18}O\text{-}NO_3^-$ values characteristic of atmospheric NO_3^-; the *dashed rectangle* delineates the expected range of nitrified $\delta^{18}O\text{-}NO_3^-$ values (−10.6 to −2.2 ‰); the *gray dashed lines* encompass mixing of atmospheric and microbially derived NO_3^-; and the two *black arrows* depict hypothetical denitrification vectors at slopes of 0.5 and 1 ($\delta^{18}O/\delta^{15}N$) (Kendall et al. 2007). The date of collection (mm-dd) is indicated on select samples. (Color figure online)

The substrate from which the N in NO_3^- originated (DOM, SOM, NH_4^+ in organic matter or minerals) and the expected range of $\delta^{15}N\text{-}NO_3^-$ values produced from nitrification ($\delta^{15}N_{nitrification}$) can be estimated by examining the $\delta^{18}N$ of the product and reactants. The only such data from our study area includes a soil sample collected from the surface organic layer at the base of an ALD and one from the scar zone of the same ALD in the PT catchment, which were analyzed for the $\delta^{15}N$ of organic N in SOM and had values of +0.2 and +1.6 ‰, respectively (Lafrenière, unpublished data). Given the limited dataset from our study area, we follow the methodology of Ansari et al. (2013) and use $\delta^{15}N\text{-}NO_3^-$ values obtained from other studies (Tye and Heaton 2007; Wynn et al. 2007) with similar potential N substrates to supplement our data and to delineate our range of $\delta^{18}N_{nitrification}$ values (between −5.8 and +7.7 ‰) (Fig. 5; Table 4). These values have been attributed to NO_3^- nitrified from substrates including snowpack NH_4^+, SOM, and NH_4^+ in clay and/or rock in European High Arctic streams (Tye and Heaton 2007; Wynn et al. 2007; Ansari et al. 2013) (Fig. 5; Table 4). Note that the $\delta^{15}N$ values of the SOM in PT are within the range reported for $\delta^{15}N$ of NH_4^+ in SOM by Tye and Heaton (2007). NH_4^+ released from N-rich sedimentary bedrock has also been shown to contribute NO_3^- in some geologic settings (Holloway et al. 1998, 2001; Holloway and Dahlgren 2002), thus NH_4^+ present in mineral soils cannot be ignored as a possibles ource of NO_3^- at this site. It should be emphasized that the $\delta^{15}N$ values in Table 4 only provide a means of constraining the most plausible, but not exact, source from which NO_3^- was derived in these watersheds.

Seasonality of streamwater NO_3^- sources

The trend in $\delta^{18}O\text{-}NO_3^-$ values in PT and GS shows that atmospheric NO_3^- was only a dominant source of streamwater NO_3^- during early melt (June 5–7; $\delta^{18}O\text{-}NO_3^-$ values from +60.3 to +81.5 ‰) (Figs. 3b, 4, 5). The $\delta^{15}N\text{-}NO_3^-$ values in runoff during the first few days of melt (−7.9 to −2.6 ‰) also sit within the range of values expected from atmospheric deposition (Fig. 3a) (Hastings et al. 2003, 2004; Heaton et al. 2004; Kendall et al. 2007). This demonstrates that in this continuous permafrost setting, the bulk ofstreamwater NO_3^- during initial melt largely results from the elution of atmospheric NO_3^- from the snowpack, as is observed in other snow-dominated catchments (Williams et al. 1995; Brooks and Williams 1999). However, lower $\delta^{18}O\text{-}NO_3^-$ values in PT from June 5 to 7 (mean = 66.6 ‰ ± 5.7) relative to mean atmospheric $\delta^{18}O\text{-}NO_3^-$ (71.4 ‰ ± 4.3, $n = 7$) and significant relationships of NO_3^- with DON and DOC in PT suggest that a proportion of NO_3^- in PT originated from nitrification or the mineralization of organic matter within the snowpack or soil surface, which is not uncommon in other permafrost regions (Wynn et al. 2007; McNamara et al. 2008; Ansari et al. 2013).

Table 4 Range of $\delta^{15}N$ signatures for potential substrates used during nitrification identified in Arctic regions

Substrate	Range of $\delta^{15}N\text{-}NH_4^+$ values (‰)	Study
Snow pack	−5.8 to −1.7	Wynn et al. (2007)
Soil organic matter	+1.2 to +2.1	Tye and Heaton (2007)
Clay and rock	−1.6 to +7.7	Wynn et al. (2007)

The more depleted $\delta^{18}O\text{-}NO_3^-$ values observed after initial discharge (−9.7 to +27.2 ‰) in both catchments indicate that the supply of NO_3^- from the snowpack was largely exhausted and that microbial mineralization and/or nitrification provided the majority of streamwater NO_3^- throughout the remainder of the season (Figs. 3b, 4, 5). Despite this change in source, concentrations of NO_3^- in GS remained near or below detection limit, signifying that consumptive processes or storage of NO_3^- in the expanding active layer outweighed NO_3^- production and continued to minimize NO_3^- export (Fig. 2b). This is not unexpected in GS given that nutrient limitation in these systems drives strong inorganic N retention (Shaver et al. 1992; Yano et al. 2010).

During stormflow, both catchments received large inputs of NO_3^- from rainfall (Louiseize and Lafrenière 2013), but the relatively low $\delta^{18}O\text{-}NO_3^-$ values in GS (13.1 to +14.6 ‰) and PT (−7.2 to −2.0 ‰) reveal that microbial NO_3^- composed upwards of 70 and 80 % of the NO_3^- in runoff in GS and PT, respectively (Fig. 4). In GS, $\delta^{15}N\text{-}NO_3^-$ values peaked and streamwater NO_3^- concentrations remained near or below detection limit despite rainfall NO_3^- concentrations between 33 and 124 ppb N (Figs. 2b, 3a); hence, much of the atmospheric NO_3^- was denitrified, assimilated by plants and/or microbes, and/or hydrologically stored within the catchment, and a small amount processed NO_3^- was flushed out of the active layer via piston flow (Figs. 4, 5). In PT, the drop in solute concentrations that occurred concomitantly with a rapid increase in discharge during the end of stormflow indicates that rainwater flowed through the system and reached the stream outlet (Fig. 2b); however, streamwater $\delta^{18}O\text{-}NO_3^-$ was at its lowest value on July 25, indicating that almost all of the NO_3^- from precipitation had been retained or recycled in the disturbed catchment as well (Figs. 3b, 4) (Burns and Kendall 2002; Campbell et al. 2002). To our knowledge, this is the first study that uses isotopic analyses to confirm nitrified or mineralized NO_3^- as the dominant source of streamwater NO_3^- following significant rainfall events in High Arctic catchments.

Impact of ALDs on NO_3^- cycling and sources

The ALDs in PT, two of which compose a long stretch of the well-carved stream channel, are potential cause for high NO_3^- export. These disturbances lack organic-rich soils, where nitrification is usually limited by strong competition/biological demand for N and where NO_3^- export is further curbed by denitrification (Giblin et al. 1991; Nordin et al. 2004; Booth et al. 2005; Yano et al. 2010; Harms and Jones 2012). The clay-rich scar zones of the ALDs limit vertical water movement (Woo and Young 2006) and channelize flow downslope (Kokelj and Lewkowicz 1998) through surficial mineral soils, which are typically characterized by larger pools of inorganic N and higher nitrification rates compared to organic soils (Nadelhoffer et al. 1991; Hobbie and Gough 2002; Harms et al. 2014). Hence, not only do the ALDs in PT limit the potential for denitrification or uptake/immobilization of NO_3^- by displacing vegetation and the organic horizon, they may also represent a source of nitrified-NO_3^-.

The effects of ALDs on NO_3^- concentrations in PT were evident since initial melt, when the peak NO_3^- concentration was twelve times higher in PT than in GS. Temporal asynchronies between NO_3^- supply and demand can fuel large NO_3^- fluxes during initial melt, and export of atmospheric NO_3^- during this time confirms that biological demand for NO_3^- was limited compared to supply in both catchments (Perakis 2002; Barnes et al. 2008; Yano et al. 2010). However in GS, low NO_3^- concentrations and enriched streamwater $\delta^{18}O\text{-}NO_3^-$ values from June 5 to 7 (mean = 77.4 ‰ ± 5.7, $n = 4$) relative to the mean atmospheric value (71.4 ‰ ± 4.3, $n = 7$) indicate that some snowpack NO_3^- was likely denitrified since the onset of melt, which is not surprising given that saturated shallow organic soils encourage denitrification and provide an effective reservoir of NO_3^- during early melt (Sickman et al. 2003; Brooks et al. 1996; Hodson et al. 2005; Harms and Jones 2012). This early biological demand for NO_3^- in GS suggests that the 12-fold higher peak NO_3^- concentration in PT likely did not simply result from a temporal disparity between NO_3^- supply and demand. Rather higher NO_3^- concentrations in PT during this time were likely enabled by the ALDs, which created a spatial discrepancy by displacing organic soils and reducing the potential for denitrification and retention via uptake or hydrological storage.

The impacts of ALDs in PT were most pronounced during stormflow. Despite higher N demand during the

growing season (Lipson and Monson 1998), which is typically between late June and mid August at CBAWO, concentrations of NO_3^- in PT peaked at 348 ppb N and were almost twice as high as rainfall concentrations due to flushing of nitrified or mineralized NO_3^- from the watershed (Figs. 2d, 3, 4). High NO_3^- export during times of high N demand in these nutrient limited systems only usually occurs when sources and sinks of NO_3^- are spatially separated from one another (Perakis 2002; Lafrenière and Lamoureux 2008). Hence, the nitrified or mineralized NO_3^- likely bypassed NO_3^- sink areas during stormflow runoff, and this led to high streamwater NO_3^- concentrations in PT. During stormflow in PT, strong negative relationships of NO_3^- with organic constituents and significant correlations of NO_3^- with Na^+ and SO_4^{2-}, which cannot be attributed to precipitation because of their low concentrations in rain but high concentration in streamwater, suggest that microbial NO_3^- was derived from mineral soils that are enriched in major ions (Table 1, 2). The ALDs are the most probable cause for the exceptionally high concentrations of microbial NO_3^- during stormflow in PT, as they provide an area where nitrified or mineralized NO_3^- can emanate from mineral soils and bypass zones of higher N demand (e.g., vegetated, organic soils) during hydrologic transport. These results are in line with those of Nowak and Hodson (2014) who reported that NO_3^- supplied from nitrification, which likely occurred in reactive sediments that were exposed due to glacier retreat, was accompanied by sulphide oxidation and therefore high concentrations of SO_4^{2-}. Our findings are also similar to those of Harms et al. (2014), who found that mineral soils provided a source of inorganic N in thermokarst gullies. The thermokarst gullies in that study also experienced less denitrification and higher rates of nitrification compared to adjacent undisturbed soils (Harms et al. 2014).

Nitrification of ammonium bound to clay particles has been shown as a source of NO_3^- in glaciated settings (Amoroso et al. 2010; Ansari et al. 2013) and provides an explanation that is consistent with enhanced export of microbially produced NO_3^- from mineral-rich scar zones in the disturbed PT catchment during stormflow. Based on the proportions of the mixing model and the mean atmospheric $\delta^{15}N\text{-}NO_3^-$ value (+1.0 ‰ ± 1.0), we would expect $\delta^{15}N$ values of the substrate to range between approximately +4.4 and +8.1 ‰ unless denitrification or uptake of NO_3^- was prominent (Wynn et al. 2007). Although we cannot affirm the substrate used during nitrification, the $\delta^{15}N$ values of nitrified-NO_3^- in PT (+4.7 to +7.3 ‰) tended to be several permil higher than the $\delta^{15}N$ of SOM from the organic and mineral soils in PT (+0.2 and +1.6 ‰) as well as those expected for NO_3^- produced from surface organic sources in other glaciated regions (e.g., +1.2 to +2.7 ‰; Table 4), which have low $\delta^{15}N$ values because of inputs from litter depleted in $\delta^{15}N$ (Högberg 1997; Tye and Heaton 2007). Values of $\delta^{15}N$ for soil N and DIN generally tend to be higher in mineral soils (Högberg 1997; Nadelhoffer et al. 1996; Kendall et al. 2007); hence it is plausible that the nitrified NO_3^- from PT originated from mineral soils in ALD scar zones.

Conclusions

This study is the first to report on and compare the seasonal dynamics and sources of NO_3^- in runoff from an undisturbed catchment (GS) and one that has been subject to a series of ALDs (PT) in a High Arctic region. Isotopic evidence indicates that NO_3^- from atmospheric deposition was only a dominant source of streamwater NO_3^- in both catchments during initial snowmelt (June 5–7) and that streamwater NO_3^- predominantly originated from microbial sources afterwards. Although both catchments shared this trend, the relative importance of NO_3^- sources and sinks differed between catchments since the beginning of melt. Low concentrations of NO_3^- and high $\delta^{18}O\text{-}NO_3^-$ values in the undisturbed catchment indicate that hydrologic storage and biological sink mechanisms in the vegetated stream channel and organic soils effectively retained or removed NO_3^- since the onset of melt. In the disturbed catchment, high NO_3^- concentrations and relatively low $\delta^{18}O\text{-}NO_3^-$ values in runoff indicate that large areas of exposed mineral soils in ALDs facilitated the export of NO_3^- from microbial sources and reduced NO_3^- retention and/or denitrification despite evidence of NO_3^- demand or storage within the catchment. $\delta^{15}N\text{-}NO_3^-$ values several permil higher than what is expected of NO_3^- derived from organic substrates and relationships between NO_3^- and major ions during times of high NO_3^- concentration suggest that mineral soils were a likely

source of the nitrified-NO_3^- in the disturbed catchment.

ALDs impacted NO_3^- export most evidently during the onset of snowmelt and especially throughout stormflow. The isotopic evidence supports that elevated export of microbial NO_3^- in the disturbed catchment was largely the result of spatial segregation between NO_3^- sources (e.g., snowmelt, mineral soils) and sinks (e.g., organic soils) created by the ALDs, which resulted in hydrological flow paths through mineral soils where N demand was likely low and nitrification was likely high relative to undisturbed soils. ALDs that are physically coupled to waterways have the potential to impact seasonal N transport by perpetuating NO_3^- export through increasing NO_3^- production and limiting NO_3^- retention.

Acknowledgments This research was funded by the Arctic Net Network of Centres of Excellence of Canada. We also extend our gratitude to the Polar Continental Shelf Program (PCSP), for exceptional logistical support. Valuable field, laboratory, and GIS assistance was provided by K. Rutherford, G. Montross, S. Montross, D Lamhonwah and A. Rudy.

References

American Society of Civil Engineers (1974) Generalized discharge relations for cutthroat flumes. J Irrig Drain Div-ASCE 98(IR4):569–583

Amoroso A, Domine F, Esposito G et al (2010) Microorganisms in dry polar snow are involved in the exchanges of reactive nitrogen species with the atmosphere. Environ Sci Technol 44:714–719

Ansari AH, Hodson AJ, Heaton THE et al (2013) Stable isotopic evidence for nitrification and denitrification in a High Arctic glacial ecosystem. Biogeochemistry 113:341–357. doi:10.1007/s10533-012-9761-9

Aravena R, Evans ML, Cherry JA (1993) Stable isotopes of oxygen and nitrogen in sources identification of nitrate from septic systems. Ground Water 31(2):180–186. doi:10.1111/j.1745-6584.1993.tb01809.x

Atkinson DM, Treitz PM (2012) Arctic Ecological classifications derived from vegetation community and satellite spectral data. Remote Sens 4:3948–3971. doi:10.3390/rs4123948

Barnes RT, Raymond PA, Casciotti KL (2008) Dual isotope analyses indicate efficient processing of atmospheric nitrate by forested watersheds in northeastern U.S. Biogeochemistry 90(1):15–27. doi:10.1007/s10533-008-9227-2

Böhlke JK, Eriksen GE, Revesz K (1997) Stable isotope evidence for an atmospheric origin of desert nitrate deposits in northern Chile and southern California, U.S.A. Chem Geol 136:135–152

Böhlke JK, Mroczkowski SJ, Coplen TB (2003) Oxygen isotopes in nitrate: new reference materials for ^{18}O:^{17}O:^{16}O measurements and observations on nitrate-water equilibration. Rapid Commun Mass Spectrom 17:1835–1846

Booth MS, Stark JM, Rastetter E (2005) Controls on nitrogen cycling in terrestrial ecosystems: a synthetic analysis of literature data. Ecol Monogr 75:139–157

Bowden WB, Gooseff MN, Balser A et al (2008) Sediment and nutrient delivery from thermokarst features in the foothills of the North Slope, Alaska: potential impacts on headwater stream ecosystems. J Geophys Res 113:G02026. doi:10.1029/2007JG000470

Brooks PD, Williams MW (1999) Snowpack controls on nitrogen cycling and export in seasonally snow-covered catchments. Hydrol Process 13:2177–2190

Brooks PD, Williams MW, Schmidt SK (1996) Microbial activity under snowpacks, Niwot Ridge, Colorado. Biogeochemistry 32(2):93–113

Buchwald C, Casciotti KL (2010) Oxygen isotopic fractionation and exchange during bacterial nitrite oxidation. Limnol Oceanogr 55:1064–1074

Burns DA, Kendall C (2002) Analyses of ^{15}N and ^{18}O to differentiate NO_3^- sources in runoff at two watersheds in the Catskills Mountain of New York. Water Resour Res 38(5):1051. doi:10.1029/2001WR000292

Campbell DH, Kendall C, Chang CCY, Silva SR (2002) Pathways for nitrate release from an alpine watershed: determination using ^{15}N and ^{18}O. Water Resour Res 38(5):1052. doi:10.1029/2001WR000294

Casciotti KL, Sigman DM, Hastings MG et al (2002) Measurement of the oxygen isotopic composition of nitrate in seawater and freshwater using the denitrifier method. Anal Chem 74(19):4905–49012. doi:10.1021/ac020113w

Cooper R, Thoss V, Watson H (2007) Factors influencing the release of dissolved organic carbon and dissolved forms of organic nitrogen from a small upland headwater during autumn runoff events. Hydrol Process 21:622–633

Favaro EA, Lamoureux SF (submitted) Antecedent Controls on Rainfall Runoff Response and Sediment Transport in a High Arctic Catchment, Geografiska Annaler, Series A: Physical Geography, GAA1405-043, submitted May 23, 2014.

Frey KE, McClelland JW (2009) Impacts of permafrost degradation on arctic river biogeochemistry. Hydrol Process 23:169–182. doi:10.1002/hyp.7196

Giblin AE, Nadelhoffer KJ, Shaver GR et al (1991) Biogeochemical diversity along a riverside toposequence. Arctic Alaska Ecol Monogr 61:415–435

Harms TK, Jones JB (2012) Thaw depth determine reaction and transport of inorganic nitrogen in valley bottom permafrost soils. Glob Change Biol 18:2958–2968. doi:10.1111/j.1365-2486.2012.02731.x

Harms TK, Abbott BW, Jones JB (2014) Thermo-erosion gullies increase nitrogen available for hydrologic export. Biogeochemistry 117:299–311. doi:10.1007/s10533-013-9862-0

Hastings MG, Sigman DM, Lipschultz F (2003) Isotopic evidence for source changes of nitrate in rain at Bermuda. J Geophys Res 108(D24):4790. doi:10.1029/2003JD003789

Hastings MG, Steig EJ, Sigman DM (2004) Seasonal variations in N and O isotopes of nitrate in snow at Summit, Greenland: implications for the study of nitrate in snow and ice cores. J Geophys Res 109:D20306. doi:10.1029/2004JD004991

Heaton THE, Wynn P, Tye AM (2004) Low 15N/14N ratios for nitrate in snow in the high arctic (79°N). Atmos Environ 38:5611–5621

Hobbie SE, Gough L (2002) Foliar and soil nutrients in tundra on glacial landscapes of contrasting ages in northern Alaska. Oecologia 131:453–462

Hodson AJ, Mumford PN, Kohler J, Wynn PM (2005) Arctic glacial ecosystems: new insights from nutrient budgets. Biogeochemistry 72:233–256

Högberg P (1997) ^{15}N natural abundance in soil-plant systems. New Phytol 137:179–203

Holloway JM, Dahlgren RA (2002) Nitrogen in rock: occurrences and biogeochemical implications. Global Biogeochem Cycles 16(4):1118

Holloway JM, Dahlgren RA, Casey WH (2001) Nitrogen release from rock and soil under simulated field conditions. Chem Geol 174:403–414

Holloway JM, Dahlgren RA, Hansen B, Casey WH (1998) Contribution of bedrock nitrogen to high nitrate concentrations in stream water. Nature 395:785–788

Jones JB, Petrone KC, Finlay JC et al (2005) Nitrogen loss from watersheds of interior Alaska underlain with discontinuous permafrost. Geophys Res Lett 32(L02401):2005. doi:10.1029/2004GL021734

Kaiser J, Hastings MG, Houlton BZ, Rockmann T, Sigman DM (2007) Triple oxygen isotope analysis of nitrate using the denitrifier method and thermal decomposition of N_2O. Anal Chem 79(2):599–607. doi:10.1021/ac061022s

Kendall C (1998) Tracing nitrogen sources and cycling in catchments, Chapter 16. In: Kendall C, Mcdonnell JJ (eds) Isotope tracers in catchment hydrology. Elsevier Science B.V, Amsterdam, pp 519–576

Kendall C, Elliott EM, Wankel SD (2007) Tracing anthropogenic inputs of nitrogen to ecosystems, chapter 12, In: Michener RH and Lajtha K (eds.) Stable isotopes in ecology and environmental science, 2nd edn, Blackwell Publishing, New York, pp. 375–449

Keuper F, van Bodegom PM, Dorrepaal E et al (2012) A frozen feast: thawing permafrost increases plant-available nitrogenin subarctic peatlands. Glob Change Biol 18: 1998–2007

Kokelj SV, Lewkowicz AG (1998) Long-term influence of active layer detachment sliding on permafrost slope hydrology, Hot Weather Creek, Ellesmere Island, Canada. In: Proceedings, seventh international conference on permafrost, yellowknife, June 2–27. Québec City Nordicana, Centre d'études nordiques, pp. 583–589.

Lafrenière MJ, Lamoureux SF (2008) Seasonal dynamics of dissolved nitrogen exports from two High Arctic watersheds, Melville Island, Canada. Hydrol Res 39(4): 323–335. doi:10.2166/nh.2008.008

Lafrenière MJ, Lamoureux SF (2013) Thermal perturbation and rainfall runoff have greater impact on seasonal solute loads than physical disturbance of the active layer. Permafrost Periglac 24(3):241–251

Lamoureux SF, Lafrenière MJ (2009) Fluvial impacts of extensive active layer detachments, Cape Bounty, Melville Island, Canada. Arct Antarct Alp Res 41(1):59–68

Levine MA, Whalen SC (2001) Nutrient limitation of phytoplankton production in Alaskan foothill lakes. Hydrobiologia 455:189–201

Lewkowicz AG, Harris C (2005) Frequency and magnitude of active-layer detachment failures in discontinuous and continuous permafrost, northern Canada. Permafrost Periglac 16:115–130

Lipson DA, Monson RK (1998) Plant-microbe competition for soil amino acids in the alpine tundra: effects of freeze-thaw and dry-rewet events. Oecologia 113:406–414

Louiseize NL, Lafrenière MJ (submitted) Active layer slope disturbances affect magnitude and composition of dissolved nitrogen export from High Arctic headwater catchments. J Hydrol HYDROL17010

McClelland JW, Stieglitz M, Pan F et al (2007) Recent changes in nitrate and dissolved organic carbon export from the upper Kuparuk River, North Slope, Alaska. J Geophys Res 112:G04S60. doi:10.1029/2006JG000371

McNamara JP, Kane DL, Hobbie JE, Kling GW (2008) Hydrologic and biogeochemical controls on the spatial and temporal patterns of nitrogen and phosphorus in the Kuparuk River, arctic Alaska. Hydrol Process 22:3294–3309. doi:10.1002/hyp.6920

Nadelhoffer KJ, Giblin AE, Shaver GR, Laundre JA (1991) Effects of temperature and substrate quality on element mineralization in six Arctic soils. Ecology 72(1):242–253

Nadelhoffer KJ, Shaver GR, Fry B et al (1996) 15 N natural abundances and N use by tundra plants. Oecologia 107: 386–394

Nordin A, Schmidt KS, Shaver GR (2004) Nitrogen uptake by soil microbes and plants in relation to soil nitrogen supply. Ecology 85(4):955–962

Nowak A, Hodson A (2014) On the biogeochemical response of a glacierized High Arctic watershed to climate change: revealing patterns, processes and heterogeneity among micro-catchments. Hydrol Process. doi:10.1002/hyp.10263

Paulter BG, Simpson AJ, McNally DJ et al (2010) Arctic permafrost active layer detachments stimulate microbial activity and degradation of soil organic matter. Environ Sci Technol 44:4076–4082

Perakis SS (2002) Nutrient limitation, hydrology and watershed nitrogen loss. Hydrol Process 16:3507–3511

Petrone KC, Jones JB, Hinzman LD, Boone RD (2006) Seasonal export of carbon, nitrogen, and major solutes from Alaskan catchments with discontinuous permafrost. J Geophys Res 111:G02020. doi:10.1029/2005JG000055

Shaver GR, Billings WD, Chapin FS et al (1992) Change and the carbon balance of arctic ecosystems. Bioscience 42: 433–441

Sickman JO, Leydecker AL, Chang CCY et al (2003) Mechanisms underlying export of N from high-elevation catchments during seasonal transition. Biogeochemistry 64: 1–24

Sigman DM, Casciotti KL, Andreani M et al (2001) A bacterial method for the nitrogen isotopic analysis of nitrate in marine and fresh waters. Anal Chem 73:4145–4153

Snider DM, Spoelstra J, Schiff SL, Venkiteswaran JJ (2010) Stable oxygen isotope ratios of nitrate produced from nitrification: 18O-labeled water incubations of agricultural and temperate forest soils. Environ Sci Technol 44: 5358–5364

Tye AM, Heaton THE (2007) Chemical and isotopic characteristics of weathering and nitrogen release in non-glacial drainage waters on arctic tundra. Geochim Cosmochim Acta 71:4188–4205

Vincent WF, Lemay M, Allard M (2013) Adapting to permafrost change: a science framework. EOS 94(42):373–375

Williams MW, Bales RC, Brown AD, Melack JM (1995) Fluxes and transformations of nitrogen in a high-elevation catchment, Sierra Nevada. Biogeochemistry 28:1–31

Woo MK, Young KL (2006) High Arctic wetlands: their occurrence, hydrological characteristics and sustainability. J Hydrol 320:432–450

Woods GC, Simpson MR, Paulter BG et al (2011) Evidence for the enhanced lability of dissolved organic matter following permafrost slope disturbance in the Canadian High Arctic. Geochim Cosmochim Acta 25:7226–7241

Wynn PM, Hodson AJ, Heaton THE, Chenery SR (2007) Nitrate production beneath a High Arctic glacier, Svalbard. Chem Geol 244:88–102. doi:10.1016/j.chemgeo.2007.06.008

Yano Y, Shaver GR, Giblin AE et al (2010) Nitrogen dynamics in a small arctic watershed: retention and downhill movement of ^{15}N. Ecol Monogr 80(2):331–351